LIMNOLOGY and OCEANOGRAPHY

ASLO

Limnol. Oceanogr. 9999, 2023, 1–16

doi: 10.1002/lno.12315

Tracing basal resource use across sea-ice, pelagic, and benthic habitats in the early Arctic spring food web with essential amino acid carbon isotopes

Kim Vane,[1*] **Matthew R. D. Cobain**,[2,3] **Clive N. Trueman**,[4] **Tobias R. Vonnahme**,[5,6] **Sebastian Rokitta**,[1] **Nicholas V. C. Polunin**,[2] **Hauke Flores**[1]

[1]Department for Biosciences, Polar Biological Oceanography, Alfred Wegener Institute for Polar and Marine Research, Bremerhaven, Germany
[2]School of Natural and Environmental Sciences, Newcastle University, Newcastle upon Tyne, UK
[3]School of Natural Sciences—Zoology, Trinity College Dublin, University of Dublin, Dublin, Ireland
[4]Ocean and Earth Science, University of Southampton, Southampton, UK
[5]Greenland Climate Research Centre, Institute of Natural Resources, Nuuk, Greenland
[6]Department of Arctic and Marine Biology, UiT—The Arctic University of Norway, Tromsø, Norway

Abstract

A rapidly warming Arctic Ocean and associated sea-ice decline is resulting in changing sea-ice protist communities, affecting productivity of under-ice, pelagic, and benthic fauna. Quantifying such effects is hampered by a lack of biomarkers suitable for tracing specific basal resources (primary producers and microorganisms) through food webs. We investigate the potential of $\delta^{13}C$ values of essential amino acids (EAAs) ($\delta^{13}C_{EAA}$ values) to estimate the proportional use of diverse basal resources by organisms from the under-ice (*Apherusa glacialis*), pelagic (*Calanus hyperboreus*) and benthic habitats (sponges, sea cucumber), and the cryo-pelagic fish *Boreogadus saida*. Two approaches were used: baseline $\delta^{13}C_{EAA}$ values, that is, the basal resource specific $\delta^{13}C_{EAA}$ values, and $\delta^{13}C_{EAA}$ fingerprints, or mean-centred baseline $\delta^{13}C_{EAA}$ values. Substantial use of sub-ice algae *Melosira arctica* by all studied organisms suggests that its role within Arctic food webs is greater than previously recognized. In addition, $\delta^{13}C_{EAA}$ fingerprints from algae-associated bacteria were clearly traced to the sponges, with an individually variable kelp use by sea cucumbers. Although mean-centred $\delta^{13}C_{EAA}$ values in *A. glacialis*, *C. hyperboreus*, and *B. saida* tissues were aligned with microalgae resources, they were not fully represented by the filtered pelagic- and sea-ice particulate organic matter constituting the spring diatom-dominated algal community. Under-ice and pelagic microalgae use could only be differentiated with baseline $\delta^{13}C_{EAA}$ values as similar microalgae clades occur in both habitats. We suggest that $\delta^{13}C_{EAA}$ fingerprints combined with microalgae baseline $\delta^{13}C_{EAA}$ values are an insightful tool to assess the effect of ongoing changes in Arctic basal resources on their use by organisms.

*Correspondence: kim.vane@awi.de

Additional Supporting Information may be found in the online version of this article.

Author Contribution Statement: K.V. and H.F. conceived the ideas and designed the methodology. K.V. collected the data. K.V. and M.C. analyzed the data and led the writing of the manuscript. M.C., C.T., T.V., S.R., P.N., and H.F. were essential in the interpretation of the very diverse nature of the data. All authors contributed critically to the drafts and gave final approval for publication.

Many organisms in the Arctic Ocean depend on ice-associated ("sympagic") algae growing inside the sea-ice brine channels or forming long-chained cell strands directly underneath the sea-ice, such as in *Melosira arctica*. Less than 20% of the total annual net primary production across the Arctic Ocean can be attributed to sea-ice algae (Hegseth 1998; Gradinger 2009; Tedesco et al. 2019), however, in some areas such as the Central Arctic Ocean, they can account for more than 50% of the primary production during summer (Gosselin et al. 1997; Fernández-Méndez et al. 2015). The early onset of the sea-ice algal bloom prior to pelagic phytoplankton blooms in the Arctic Ocean can play a critical role in zooplankton life cycles (Leu et al. 2011; Wang et al. 2015). Key Arctic species

such as the pelagic copepod *Calanus* spp. and polar cod *Boreogadus saida* are partly dependent on sea-ice algae (Søreide et al. 2006, 2008; Budge et al. 2008; Wang et al. 2015; Kohlbach et al. 2016, 2017). Polar cod, as the main consumer of Arctic under-ice zooplankton, transfers up to 75% of the total organic carbon to higher trophic levels such as seabirds, seals, and polar bears (Welch et al. 1992; Darnis et al. 2012). The rapidly sinking sea-ice algae at the retreating sea-ice margin in early spring are also critical for the benthic faunal production (Wassmann et al. 2006; Budge et al. 2008; Tamelander et al. 2008; Boetius et al. 2013). Therefore, the bloom timing of sea-ice and pelagic microalgae during spring and summer is an important driver of Arctic ecosystem productivity.

The growth dynamics of Arctic sea-ice algae and pelagic phytoplankton are expected to undergo major changes, as the region is warming at twice the global average rate (Cohen et al. 2014). The resulting sea-ice decline (i.e., the thinning, northward retreat and shortening seasonal coverage) is likely to amplify Arctic warming, and an ice-free Arctic is expected by the mid-20th century (Notz and Stroeve 2018). Although thinner sea-ice may temporarily promote ice-algal production in some regions (Tedesco et al. 2019), negative effects on sea-ice algae production are anticipated in the long term (Lannuzel et al. 2020). Younger and thinner sea-ice with variable snow cover can cause higher light penetration and stress, with higher temperatures leading to less regular sea-ice algal growth (Ji et al. 2013; Lange et al. 2019; Kvernvik et al. 2020). Apart from the under-ice fauna, benthic communities on the Arctic continental shelves can be significantly affected due to their reliance on rapidly sinking sea-ice algae with sea-ice retreat in early spring (Tamelander et al. 2008). Lower sea-ice algae contribution to the benthic communities might not be offset by an increase in pelagic phytoplankton biomass due to potentially enhanced pelagic zooplankton feeding rates preventing the microalgal biomass from reaching the sea floor (Ji et al. 2013; Grebmeier et al. 2018).

The consequences of a reduced sea-ice algae contribution to Arctic ecosystem productivity are not well understood due to the lack of studies across seasons and locations (Kędra et al. 2015). Determining the influence of changing basal resources on benthic faunal productivity at the marginal Arctic sea-ice zone is complicated due to the additional contributions of macroalgae and other microorganisms (bacteria and fungi) in the water column or sediment. Characterizing a wide range of basal resources with biomarkers, such as fatty acids and bulk isotopes, to estimate their subsequent use by heterotrophic organisms is challenging; what is needed is characterization of many basal resources with enough distinction to trace them through food webs. Microorganisms are often not characterized due to the difficulty of extracting them directly from the field in sufficient biomass for isotope analysis. Bulk stable isotopes mostly distinguish between sea-ice algae and pelagic phytoplankton due to their large difference in $\delta^{13}C$ values (Tamelander et al. 2009; de la Vega et al. 2019). However, the large ranges in bulk $\delta^{13}C$ values associated with variation in the carbon isotope composition of the environmental substrate and differential carbon fractionation reduce discrimination among other primary producers during photosynthetic fixation. This complicates the tracing of basal resource use over spatiotemporal scales. Estimates of basal resource use from bulk isotope analysis are further complicated by the integration of all tissue macromolecules, that is, lipids, proteins, carbohydrates, which undergo varying carbon fractionation with each step in the trophic chain. Fatty acid profiles can distinguish between dinoflagellates and diatoms, which can be traced to their under-ice or pelagic origin with the $\delta^{13}C$ values of essential fatty acids (Budge et al. 2008; Kohlbach et al. 2016, 2017). However, the taxonomic resolution of a large range of simultaneously detectable basal resources remains limited with fatty acids (Ruess and Müller-Navarra 2019).

Compound-specific analysis of carbon isotopes in EAAs has shown potential to characterize specific primary producers as well as microorganisms (Larsen et al. 2009, 2012, 2013). As a likely consequence of different carbon isotopic fractionations during potentially variable EAA biosynthetic pathways across basal resources, the $\delta^{13}C$ values of individual EAAs ($\delta^{13}C_{EAA}$ values) can be used to identify specific basal resources (Larsen et al. 2009). Although underlying mechanisms are poorly understood (Besser et al. 2022), discrimination among major taxa, such as bacteria, plants, microalgae, and their clades, has been observed by centering individual $\delta^{13}C_{EAA}$ values to the mean $\delta^{13}C_{EAA}$ value within samples of basal resources that creates a suite of relative $\delta^{13}C$ values of EAAs, that is, $\delta^{13}C_{EAA}$ patterns (Larsen et al. 2009, 2012). The $\delta^{13}C_{EAA}$ patterns in autotrophs remain consistent despite spatiotemporal changes in environmental factors, including $\delta^{13}C$ values of dissolved inorganic carbon, pH, salinity, and temperature that can alter the baseline $\delta^{13}C_{EAA}$ values of basal resources (Larsen et al. 2013, 2015; Lynch et al. 2016; Elliott Smith et al. 2022). The mean-centring of baseline $\delta^{13}C_{EAA}$ values shows the relative carbon fractionation during EAA biosynthesis and removes the variability in basal resource baseline $\delta^{13}C_{EAA}$ values associated with $\delta^{13}C$ values of inorganic sources and physical and chemical factors. The $\delta^{13}C_{EAA}$ patterns can therefore be characterized from basal resources grown in laboratory cultures (e.g., microalgae, bacteria, and fungi) as well as those sampled in the field (Scott et al. 2006; Larsen et al. 2009). Specific $\delta^{13}C_{EAA}$ patterns that are unique and distinctive within a specific basal resource group or clade are referred to as $\delta^{13}C_{EAA}$ fingerprints. As metazoans cannot synthesize EAAs de novo, they must be assimilated from their diet, during which feeding studies have observed negligible carbon isotope fractionation of the EAA carbon skeleton (McMahon et al. 2010, 2015; Wang et al. 2018). Therefore, basal resource use by metazoans can be traced throughout the food web by comparing $\delta^{13}C_{EAA}$ patterns in metazoan tissues to $\delta^{13}C_{EAA}$ fingerprints associated with specific basal resource clades.

In this study, we explore the utility of $\delta^{13}C_{EAA}$ values for estimating the proportional use of specific and diverse basal resources by Arctic organisms in the northern Barents Sea and the adjacent Arctic Ocean. Well-known Arctic invertebrates from the under-ice (*Apherusa glacialis*), pelagic (*Calanus hyperboreus*), and benthic (sponge, sea cucumber) habitat, and the cryo-pelagic polar cod (*B. saida*), were collected at the onset of sea-ice melt in early Arctic spring. These organisms represent the breadth of known intermediate trophic-level functional groups, covering under-ice zooplanktonic herbivory, pelagic zooplanktivory, detritivory, and filter feeding. The specificity with which Arctic basal resources can be traced and characterized across these ecologically diverse consumers and habitats is assessed through the use of Bayesian mixing models, comparing the $\delta^{13}C_{EAA}$ patterns in opportunistically field-collected basal resources and cultured microorganisms with those in the tissues of Arctic organisms.

Materials and methods

In situ sample collection

Field samples were collected during the RV *Polarstern* expedition PS106/2 from 23 June to 20 July 2017 on the Barents Sea and the Nansen Basin between 78°N and 84°N, covering an area of about 700 × 2800 km (Fig. 1). Ice-associated particulate organic matter (iPOM; representing the sympagic ice algae community), was collected by taking four ice cores at two sites with a 9 cm interior diameter ice corer and one sample directly under the ice surface. The bottom 5 cm of the four ice cores were defrosted in sterile filtered seawater in the dark at 4°C on board of the ship. Seven pelagic particulate organic matter (pPOM; representing the pelagic phytoplankton community) samples were taken with Niskin bottles in a Niskin/CTD rosette at six stations at ~ 10 m depth. Both iPOM and pPOM samples (300 mL and 2–9 L of water, respectively) were filtered with a vacuum pump onto precombusted 0.7 μm GF/F filters with 47 mm diameter and stored at −20°C.

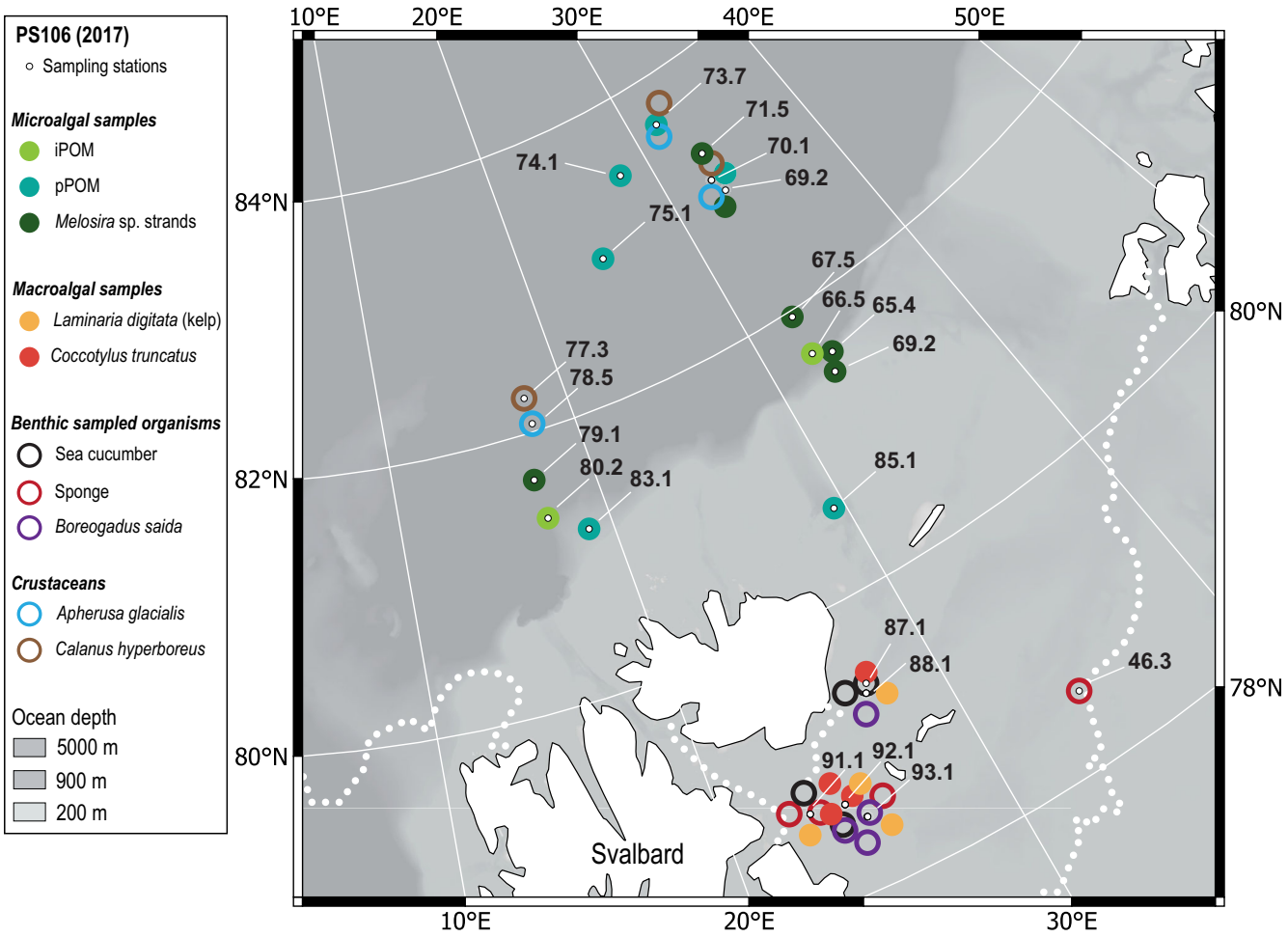

Fig. 1. Map of the sample locations of each organism and field-collected basal resources during the PS106 in 2017. Benthic trawl station 46.3 was sampled first on 27 June, with the under-ice stations 65.4–79.1 on 01–13 July before returning to benthic trawls at stations 88.1–93.1 until 17 July where the sea-ice cover disappeared 2 weeks before. The boundary of the area with at least 15% sea-ice coverage on 01 July 2017 was indicated with a white dotted line.

A Surface-Under-Ice-Trawl (SUIT; Van Franeker et al. 2009) equipped with a 7 mm shrimp net and a 0.15 mm mesh mesozooplankton net was used to collect copepods *C. hyperboreus*, ice amphipods *A. glacialis*, and sub-ice algal strands composed primarily of *M.* arctica up to 2 m below the sea-ice. One sample of *C. hyperboreus* was taken with a Rectangular-Midwater-Trawl (RMT) at 200-m depth at Sta. 77.3 (Fig. 1). Bottom trawls deployed to a depth of 110–300 m with a 20 cm mesh size sampled polar cod *B. saida* (between 9 and 22 cm TL), sponges (species unknown), sea cucumbers (likely *Molpadia* sp.), red macroalgae *Coccotylus truncates*, and the kelp *Laminaria digitata*. The area of the bottom trawls was covered by sea-ice approximately 2 weeks before the sampling of the benthic organisms (*see* Fig. 1). Sampling with SUIT and RMT nets was conducted in ice-covered waters.

Cultured basal resource taxa

The sea-ice bacterium, *Marinomonas primoryensis* was isolated from sea-ice algal enrichments of primarily *Nitzschia frigida* in the lowermost (0–3 cm) skeletal layer of sea-ice sampled with an ice corer (9 cm inner diameter) in van Mijenfjorden, Svalbard. The skeletal layer was melted in the dark with nutrient-enriched sterile filtered seawater. Two other bacterial strains, *Pseudoalteromonas arctica* and *Pseudoalteromonas elyakovii* were isolated from phytoplankton net hauls that were dominated by the diatom *Chaetoceros socialis* (0–30 m with a 20 μm mesh size phytoplankton net) in Kaldfjorden, Tromsø. A detailed description of bacterial strain isolation and identification is described by Vonnahme et al. (2021).

All bacteria strains were then cultured in triplicate on an amino acid (AA) free MAG medium as described in Larsen et al. (2009) for approximately 4 weeks until sufficient biomass accumulated. Three species of marine Arctic fungi, *Sarocladium strictum*, *Oblongichytrium* sp., and *Sphaeroforma napiecek* (Bering Sea) were grown in triplicate on a Modified Melin-Norkrans medium as described in Larsen et al. (2009) for approximately 4 weeks. Cultures of the Arctic sea-ice algae *Navicula* sp., *M. arctica*, and *Thalassiosira* sp., and the pelagic phytoplankters *Thalassiosira hyalina* and *Micromonas pusilla* were grown in triplicates in sterile filtered (2 μm; Sartobran 300 capsule filter; Sartorius) Arctic seawater at a salinity of $\sim$ 33 and a temperature of $\sim$ 0°C. The filtered Arctic sea water was enriched with vitamins and trace metals according to the F/2 recipe (Guillard and Ryther 1962), and nitrate and phosphate were added in concentrations of 100 and 6 μmol L^{-1}, respectively. Cells of each microalgae species were harvested onto precombusted (500°C, 10 h) glass fiber filters (GF/F; Whatman) and stored at −20°C.

Stable isotope analysis

Fish muscle tissue (1 mg), sea cucumber body wall tissue (2 mg), sponge tissue (2 mg), individual whole zooplankton (1 mg), *M. arctica* strands (2 mg), and all GF/F filters were freeze-dried and homogenized. Individual samples were then hydrolysed after addition of the internal reference 6-aminocaproic acid in 6 mol L^{-1} HCL for 20 h at 110°C. The acid was evaporated in a heating block at 80°C under a nitrogen flow, and the samples were purified with a cation exchange resin (DOWEX 50WX8, 100–200 mesh, hydrogen form). After DOWEX purification, the remaining fine GF/F filter material was removed with a 0.45 μm PTFE disc filter with 0.01 mol L^{-1} HCl and the AA sample was again dried in a heating block. The dry AA samples were redissolved in 100 μL of 0.1 mol L^{-1} HCL, and 35 μL of methanol, 30 μL of pyridine, and 15 μL of methylchloroformate were added, after which the sample was left for 5 min to react (Walsh et al. 2014). After an addition of 100 μL of chloroform, AAs were extracted from the bottom organic layer consisting of chloroform.

The $\delta^{13}C$ values in AAs were measured on a Delta V Plus mass spectrometer interfaced to a Thermo 1310 GC Isolink/Conflo IV gas chromatograph through a GC-C III interface. Samples were injected in splitless mode onto a Stabilwax column (60 m, 0.25 mm ID, 0.25 μm film thickness). All samples were injected in triplicate, but injection volumes differed between samples due to the large variation in AA concentration and compositions. The GC program utilized was 60°C (2 min), increased with 3°C s^{-1} to 245°C, and held for 45 min. An in-house standard consisted of nine pure AAs purchased from Sigma-Aldrich and four internationally available AAs, phenylalanine, alanine, methionine, and leucine from SI Science Co. We assessed eight replicate runs of the AA standard at the beginning, mid and end of the analysis period, to calculate the long-term analytical standard deviation of each EAA. These were incorporated in the mixing model trophic discrimination factor (TDF) to account for the individual variability of $\delta^{13}C_{EAA}$ values across the analytical period where sample were run (*see* Table S1). Six EAAs, valine (Val), isoleucine (Iso), leucine (Leu), threonine (Thr), phenylalanine (Phe), lysine (Lys), were consistently measured with sufficient baseline separation and peak height. The average precision of AA methoxycarbonyl esterification is comparable to other derivatization methods despite the non-uniform high recoveries for AAs with polar or charged side chains (Walsh et al. 2014). Thus, all measured $\delta^{13}C_{EAA}$ values were corrected for kinetic fractionation during derivatization according to the mass balance equation described by Docherty et al. (2001).

Data analysis

We present and analyze the $\delta^{13}C_{EAA}$ values in two ways: the baseline $\delta^{13}C_{EAA}$ values, that is, the measured $\delta^{13}C_{EAA}$ values of the six EAAs after correction for kinetic fractionation during derivatization, and $\delta^{13}C_{EAA}$ patterns, that is, a collective term for the suite of the six baseline $\delta^{13}C_{EAA}$ values that were individually centred to the mean baseline $\delta^{13}C_{EAA}$ values of all six EAAs in each sample. Baseline $\delta^{13}C_{EAA}$ values are a product of the primary producers at the base of the food web,

Table 1. The averages and standard deviation of the six mean-centred $\delta^{13}C_{EAA}$ values that comprise the $\delta^{13}C_{EAA}$ patterns in each basal resource and consumer tissues used in the mixing model.

	N	Val	Ile	Leu	Thr	Phe	Lys
Basal resources							
iPOM	5	3.6±0.8	−1.8±0.9	9.2±1.2	−10.9±1.2	6.0±1.3	−6.1±0.7
pPOM	7	4.2±0.5	−1.4±0.4	7.6±1.3	−9.5±1.0	5.5±0.8	−6.5±0.8
Melosira sp.	6	3.6±0.4	−4.7±0.5	4.7±1.4	−6.7±1.7	4.6±0.8	−1.5±0.8
Kelp (*Laminaria digitata*)	4	3.7±0.9	−0.1±0.4	6.2±0.3	−12.8±2.3	7.1±0.5	−4.1±0.5
Red macroalgae (*Coccotylus truncatus*)	4	−0.3±0.2	−1.3±0.6	0.8±1.4	1.8±1.0	3.6±0.1	−4.7±0.2
Bacteria	8	0.4±1.4	0.4±0.8	1.7±2.4	−6.1±2.1	6.9±2.0	−3.3±1.3
Fungi	9	−2.2±0.6	0.4±1.7	5.4±1.6	−8.1±2.8	6.0±1.7	−1.5±1.6
Consumers							
Apherusa glacialis	9	3.4±0.5	−3.8±0.6	7.6±0.6	−9.0±1.0	7.7±0.7	−5.7±0.6
Boreogadus saida	10	3.1±0.9	−2.9±0.8	6.9±1.0	−9.2±2.1	7.2±0.7	−5.2±0.7
Calanus hyperboreus	9	3.5±0.6	−4.0±0.3	6.4±1.3	−7.8±1.4	6.9±1.2	−5.1±0.6
Sea cucumber	7	2.5±0.6	−1.7±1.0	6.3±1.1	−9.5±2.8	6.2±1.2	−3.8±1.0
Sponge	5	2.5±0.9	−1.2±0.6	3.7±1.3	−7.2±1.0	4.1±0.4	−2.0±1.0

Table 2. The averages and standard deviation of the six baseline $\delta^{13}C_{EAA}$ values in each basal resource and consumer tissues used in the mixing model.

	N	Val	Ile	Leu	Thr	Phe	Lys
Basal resources							
iPOM	5	−25.4±2.3	−20.1±2.4	−31.0±2.2	−10.9±3.0	−27.9±2.4	−15.8±1.5
pPOM	7	−33.1±2.1	−27.4±2.5	−36.4±2.7	−19.3±2.9	−34.4±1.8	−22.4±2.5
Melosira arctica	6	−26.1±1.2	−17.7±1.1	−27.2±1.5	−15.7±2.1	−27.0±1.2	−20.9±1.4
Consumers							
Apherusa glacialis	9	−26.4±1.2	−19.1±1.2	−30.4±0.8	−13.9±1.3	−30.7±1.4	−17.2±1.0
Boreogadus saida	10	−25.7±2.3	−19.7±2.0	−29.5±2.3	−13.4±3.2	−29.7±2.2	−17.4±2.2
Calanus hyperboreus	9	−29.9±1.6	−22.4±1.6	−32.7±1.5	−18.5±2.6	−33.2±1.8	−21.2±1.8

resulting from the combination of (1) environmental factors that includes $\delta^{13}C$ values of dissolved inorganic carbon subject to seasonal, physical, and chemical variability, and (2) the carbon fractionation during chemo- or photosynthesis and EAA synthesis pathways. In contrast, the mean-centring of the baseline $\delta^{13}C_{EAA}$ values to $\delta^{13}C_{EAA}$ patterns removes this environmental variability by focusing on the relative differences between individual $\delta^{13}C_{EAA}$ values. Through mean-centring, $\delta^{13}C_{EAA}$ patterns reflect consistent differences in the carbon fractionation during individual EAA biosynthesis and means that $\delta^{13}C_{EAA}$ patterns are comparable between most field and cultured samples. The $\delta^{13}C_{EAA}$ patterns are considered $\delta^{13}C_{EAA}$ fingerprints for basal resources when they are distinguishable from other basal resource $\delta^{13}C_{EAA}$ patterns. With negligible alterations of baseline $\delta^{13}C_{EAA}$ values from basal resources to consumer in EAAs (McMahon et al. 2010; Wang et al. 2018; Takizawa et al. 2020), $\delta^{13}C_{EAA}$ patterns produced by basal resources also remain preserved in animal tissues as they are assimilated and transfer through the food web. Animal tissue $\delta^{13}C_{EAA}$ patterns will therefore reflect a relative mixture of the basal resource $\delta^{13}C_{EAA}$ patterns used to synthesize their tissues.

The $\delta^{13}C_{EAA}$ fingerprints of basal resources are the most powerful discriminators to characterize specific basal resource taxa or clades by enabling the use of both field-collected and cultivated primary producers and microorganisms. Therefore initially, we graphically explored $\delta^{13}C_{EAA}$ patterns with principal component analysis (PCA; R: vegan) and pairwise EAA plots (biplots) to determine whether (1) the $\delta^{13}C_{EAA}$ patterns in sampled basal resources presented distinctive $\delta^{13}C_{EAA}$ fingerprints, and (2) if consumer tissue $\delta^{13}C_{EAA}$ patterns were contained within the $\delta^{13}C_{EAA}$ pattern space of the basal resources, a key requirement to statistically estimate resource contributions with mixing models. We observed that iPOM and pPOM samples expressed similar $\delta^{13}C_{EAA}$ patterns and that only the sea cucumber and sponge tissue $\delta^{13}C_{EAA}$ patterns were fully enclosed within the basal resource $\delta^{13}C_{EAA}$ pattern space. Thus, to estimate proportional basal resource

contributions to the benthic consumers, we used Bayesian mixing models (R: MixSIAR) on the six mean-centred $\delta^{13}C_{EAA}$ values that comprise the $\delta^{13}C_{EAA}$ patterns, run separately for sponges and sea cucumber. Mixing models were constructed with only individual random effects as drivers in basal resource use, due to the limited sample replication and distance between sampling sites (*see* Fig. 1) for these consumers. As iPOM and pPOM $\delta^{13}C_{EAA}$ patterns were similar, model estimates of contributions for these two basal resources were combined post hoc into a single microalgae group, following mixing model recommendations of Phillips et al. (2014).

For the pelagic-sympagic consumers (*A. glacialis*, *C. hyperboreus*, and *B. saida*), tissue $\delta^{13}C_{EAA}$ patterns aligned exclusively with those of the microalgae (iPOM, pPOM, and *M. artica*) on the boundary of, but not fully enclosed within the total basal resource $\delta^{13}C_{EAA}$ pattern mixing space. We therefore turned to baseline $\delta^{13}C_{EAA}$ values, which excludes the use of cultured bacteria and fungi resources for estimating basal resource contributions. Significant contributions of macroalgal sources were excluded a priori due to the extensive stomach content analyses of *B. saida* in the region suggesting polar cod are essentially wholly reliant on pelagic and sympagic zooplankton (Eriksen et al. 2020). Therefore, iPOM, pPOM, and *M. arctica*, which had distinctive baseline $\delta^{13}C_{EAA}$ values, were the only basal resources considered in the mixing model. Bayesian mixing models were constructed separately for each species. For *A. glacialis* and *C. hyperboreus*, potential spatial variation in basal resource use was explored by considering individual nested within sampling stations as random effects. For polar cod, we considered size class (small or large demarcated at 15 cm total length) as a potential driver of individual resource use. The importance of these potential drivers was assessed by comparing model deviance information criterion (DIC), which provides an indication of relative information loss of models given their complexity, and leave-one-out cross-validation information criterion (LOOic), which gives a measure of the out-of-sample predictive fit (Stock et al. 2018). The Akaike weights, which quantify the proportional support for competing models given LOOic values, were also calculated.

The Bayesian framework of these mixing models allows the incorporation of known uncertainties when estimating basal resource contributions, including the observed spread in $\delta^{13}C_{EAA}$ values for basal resource groups. For mixing models using $\delta^{13}C_{EAA}$ values data, TDFs, or the average change in $\delta^{13}C_{EAA}$ values between a consumer and its diet specific to each EAA, are often set to 0.1 or 0.4 for all EAAs. This stems from the negligible deviations expected and observed between diet and consumer tissue $\delta^{13}C_{EAA}$ values in controlled feeding studies (McMahon et al. 2010, 2015; Wang et al. 2018), which contrasts with significant TDFs observed in bulk stable isotopes (e.g., Sweeting et al. 2007). While it is unlikely that TDFs will be homogenous for all EAAs, such small TDFs will in general not account for the large variations displayed by the consumer tissue $\delta^{13}C_{EAA}$ patterns and baseline $\delta^{13}C_{EAA}$ values, spanning almost 20% within groups across the six EAAs (*see* Tables 1, 2). These generic, small TDFs will therefore have limited impact on the estimated proportions of basal resource use. Conversely, analytical variation in $\delta^{13}C$ values can be very distinct for individual EAAs and can only be observed when they are assessed over the entire analytical period where basal resource and tissue samples were measured. This can be due to the differential behavior of certain EAAs in the analytical instrument. While the measurements during triplicate injections are indicative of daily analytical accuracy, the long-term analytical deviations are better represented by the AA standard run throughout the entire analytical period. We, therefore, did not explicitly incorporate variability associated with TDFs into our mixing models, but instead incorporated the analytical measurement error for each AA, as determined from standard reference materials (*see* Table S1), as a source of uncertainty across all models.

All Bayesian mixing models were run with three chains for 1×10^6 iterations, with a burn-in of 5×10^5 and a thinning of 500. This resulted in model parameters, including proportion contributions of each basal resource, being estimated as posterior distributions constructed from 3000 sample draws, from which posterior means, medians and credible intervals were calculated. Model convergences were checked using the Geweke and Gelman diagnostics. For more detailed descriptions of Bayesian mixing model approaches, including model formation, assumptions, error structures and best practices, we refer readers to Parnell et al. (2010); Phillips et al. (2014); and Stock et al. (2018). All analyses were conducted in R version 4.0.5 (R Core Team 2018) implemented via RStudio version 1.4.1106, using the package "MixSIAR" (version 3.1.12; Stock et al. 2018).

Results

Using $\delta^{13}C_{EAA}$ patterns to estimate basal resource use for Arctic consumers

Benthic macroalgae, cultured fungi and bacteria, and field-collected *M. arctica* strands could be distinguished by their $\delta^{13}C_{EAA}$ patterns, therefore can be considered $\delta^{13}C_{EAA}$ fingerprints (Figs. 2A, 3; Table 1). Although the PCA does not show a clear separation of the bacterial and fungal resources based on PC1 and PC2 scores for $\delta^{13}C_{EAA}$ patterns, separation between bacterial and fungal sources is expressed on PC4, accounting for 7.3% of the variability (*see* Fig. S4), mostly driven by mean-centred $\delta^{13}C$ values of valine. The three seemingly outlying fungal data points are the three replicate measurements of *Oblongichytrium* sp. (Figs. 2A, 3). The $\delta^{13}C_{EAA}$ patterns derived from the iPOM and pPOM filters showed considerable overlap in PCA space and similar mean-centred $\delta^{13}C$ values across all six EAAs (Table 1). The iPOM and pPOM filtrates were therefore not considered to have distinctive $\delta^{13}C_{EAA}$ fingerprints (Figs. 2A, 3). Consequently, they were

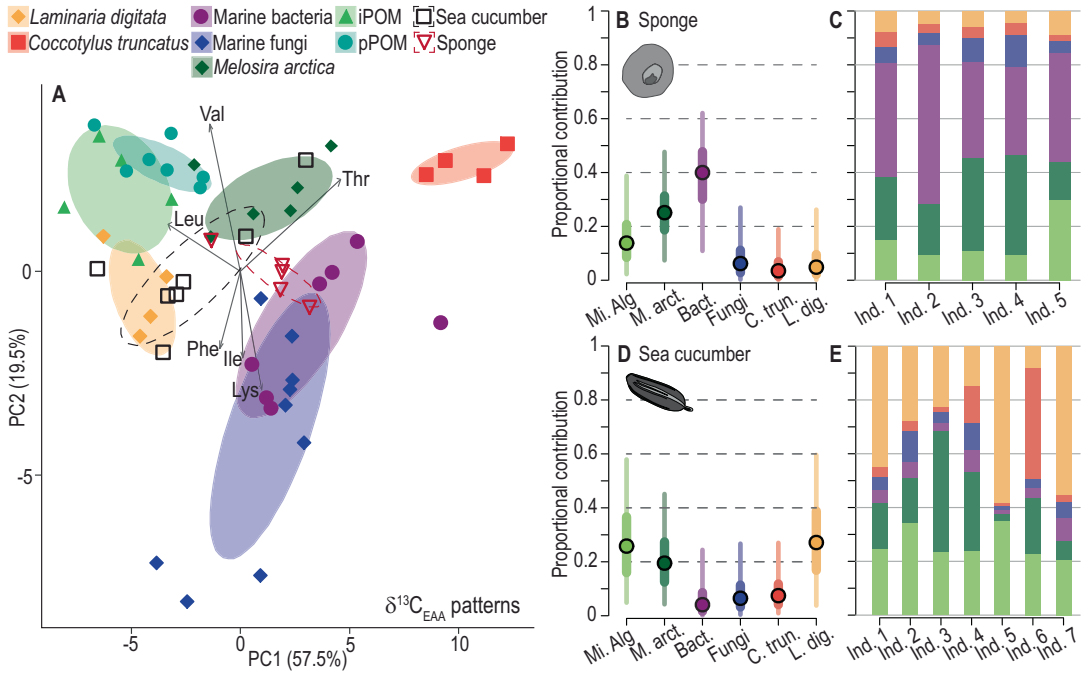

Fig. 2. Principal component analysis of the six individual mean-centred $\delta^{13}C_{EAA}$ values that comprise the $\delta^{13}C_{EAA}$ patterns in all basal resources compared to sponge and sea cucumber individuals (**A**). Ellipses represent 60% of the data. Population average basal resource utilization estimated through mixing models using the six mean-centred $\delta^{13}C_{EAA}$ values are plotted for sponge (**B**) and sea cucumber (**D**) as the posterior median (point), 50% (dark colored, wide band) and 95% (light colored, thin band) credible intervals for each basal resource. Individual variability in basal resource utilization by sponge (**C**) and sea cucumbers (**E**) are shown as stacked barplots of mean basal resource contributions estimated for each individual. Note that iPOM and pPOM are combined post hoc as a microalgal group (Mi. Alg).

grouped together in mixing model proportional estimates post hoc as a single microalgae resource group for models based on $\delta^{13}C_{EAA}$ patterns (Fig. 2B–E).

Consumers from the benthic habitats, sea cucumbers and sponges, were well contained within the $\delta^{13}C_{EAA}$ pattern mixing space defined by the basal sources (Fig. 2A). Sea cucumber $\delta^{13}C_{EAA}$ patterns showed larger variation among individuals than in sponge individuals (as demonstrated by their larger ellipse area in Fig. 2A). This was consistent with mixing model output for these species; the standard deviation of the individual random effect on basal resource use estimated for sea cucumbers (mean of 1.78, 95% credible intervals from 0.88 to 3.74) was greater than that of sponges (0.99, 0.09–3.09). Overall, mixing models estimated marine bacteria as the dominant contributor to sponge basal resource use, reaching up to 58% for individual 3 (Fig. 2B,C), with *M. arctica* strands and microalgae also each making significant contributions of over 10% on average (Fig. 2B). Conversely, mixing models estimated similar contributions of *M. arctica* and microalgae to the average sea cucumber diet (Fig. 2D), although variability between individuals was apparent, especially for *M. arctica* (Fig. 2E). Kelp (*L. digitata*) was also suggested to be a major basal resource for sea cucumbers with contributions up to 60% (Fig. 2E).

The $\delta^{13}C_{EAA}$ patterns of *A. glacialis*, *C. hyperboreus*, and *B. saida* did not wholly fall within the mixing space of the sampled basal resources (Fig. 3). However, their $\delta^{13}C_{EAA}$ patterns showed the highest similarity to iPOM/pPOM filtrates and *M. arctica*, while their dissimilarity in $\delta^{13}C_{EAA}$ patterns with marine bacteria and fungi suggests little to no contribution of these sources (Fig. 3). Pairwise EAA biplots indicated that the deviation of $\delta^{13}C_{EAA}$ patterns in these animal tissues from those of the basal resources was predominantly caused by higher mean-centred phenylalanine $\delta^{13}C$ values (Fig. S2; Table 1), which had the lowest weighting of EAAs in PC1 and PC2 (Fig. 3). Therefore, $\delta^{13}C_{EAA}$ patterns were not considered for mixing models with these consumers.

Tracing Arctic microalgal resources with baseline $\delta^{13}C_{EAA}$ values

Although similar in their $\delta^{13}C_{EAA}$ patterns, iPOM and pPOM samples separated in their baseline $\delta^{13}C_{EAA}$ values and were also distinct from *M. arctica* strands (Fig. 4A; Table 2). Their variability across all six EAA tracers captured those of the baseline $\delta^{13}C_{EAA}$ values in *A. glacialis*, *C. hyperboreus*, and *B. saida* (Fig. 4A and *see* EAA biplots Fig. S2). Mixing models based on baseline $\delta^{13}C_{EAA}$ values for both *A. glacialis* and *C. hyperboreus* supported the inclusion of site as a random effect (Akaike weights of 82% and 94%, respectively; Table 3). For polar cod, greatest support was given to the model which included individual random effects only (66%), although size

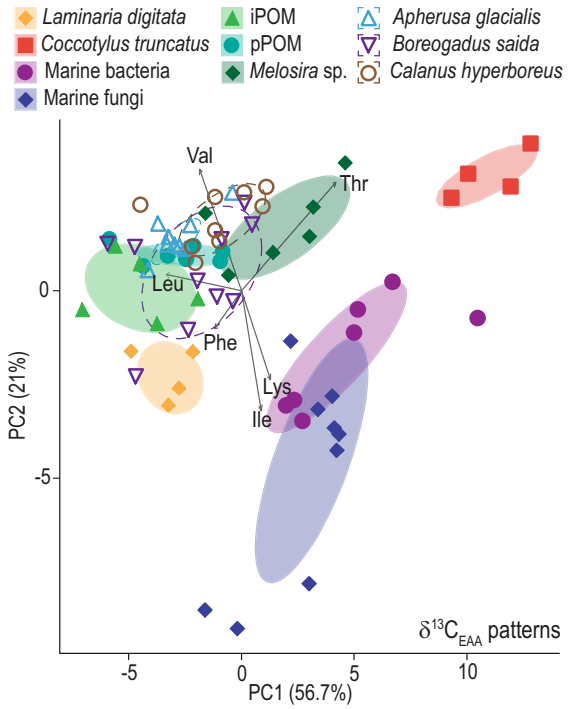

Fig. 3. Principal component analysis of the six individual mean-centred $\delta^{13}C_{EAA}$ values that comprise the $\delta^{13}C_{EAA}$ patterns in all basal resources compared to those in in the tissues of two crustaceans, *Apherusa glacialis* and *Calanus hyperboreus*, and polar cod, *Boreogadus saida*. Ellipses represent 60% of the data.

cannot be fully excluded given the similarity in the leave-one-out information criterion and their large standard errors (Table 3).

Mixing models estimated that iPOM had the highest proportional contributions to EAAs in tissues of the under-ice amphipod *A. glacialis* across sites and individual polar cod *B. saida*, and least for the pelagic copepod *C. hyperboreus* (Fig. 4B–D). Spatial differences in basal resource use were overall more apparent in *C. hyperboreus* with median estimated pPOM contributions varying from 36% to 78% between sites, whereas for *A. glacialis* median pPOM contributions ranged from 10% to 22% (Fig. 4B,C). However, for both species, differences between sites were greater than those attributed to individual variation within sites. Mean ratios of site to individual random effect standard deviations were 2.65 for *A. glacialis* and 4.02 for *C. hyperboreus*, with little differences estimated between individuals within sites (*see* Fig. S5). For both *A. glacialis* and *C. hyperboreus*, the estimated proportional contribution from iPOM decreased while contributions from pPOM increased from station 70.2 to stations 78.5 and 77.3, respectively (Fig. 4B,C). Stations 77.3 and 78.5 were close to each other and located further southwest in more open water compared to stations 70.1 and 73.7 (*see* Fig. 1). Polar cod individuals displayed considerable variability in apparent basal resource use, with a minimal effect of body size class (Fig. 4E;

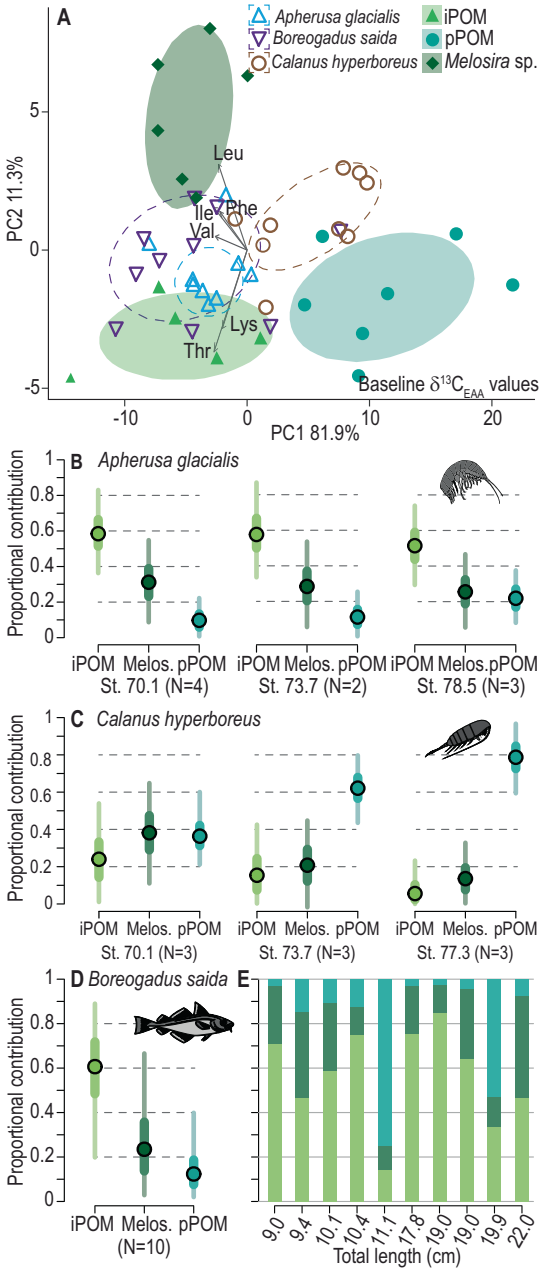

Fig. 4. Principal component analysis (**A**) of the six baseline $\delta^{13}C_{EAA}$ values in iPOM, pPOM, and *Melosira arctica* strands compared to those of the tissues in crustaceans *Apherusa glacialis*, *Calanus hyperboreus*, and polar cod, where the ellipses represent 60% of the data. Estimated site average partitioning through mixing models using the six baseline $\delta^{13}C_{EAA}$ values of the aforementioned basal resources for *A. glacialis* (**B**) and *C. hyperboreus* (**C**), and population average basal resource partitioning for *Boreogadus saida* (**D**) are plotted as the posterior median (point), 50% (dark colored, wide band) and 95% (light colored, thin band) credible intervals for each source. Individual variability in basal resources for *B. saida* (**E**) are shown as stacked barplots of mean basal resource contributions estimated for each individual denoted by their measured total body length. Overall average and individual basal resource variability for *A. glacialis* and *C. hyperboreus* are provided in Fig. S5.

Table 3. Comparison of mixing models for pelagic consumers, with model support determined by lower deviance information criterion (DIC) and leave-one-out cross-validation information criterion (LOOic, plus standard error, SE). Relative model support is given as Akaike weights that sum to one across nested models. Note that size class is fitted as fixed effect whereas site and individual are fitted as random effects (individual nested within site).

Species	Model	DIC	LOOic	SE (LOOic)	Akaike weight
Apherusa glacialis	1|site:Individual	64.0	45.7	9.5	0.82
	1|individual	72.2	48.7	11	0.18
Calanus hyperboreus	1|site:Individual	76.7	60.0	7.7	0.94
	1|individual	80.4	65.5	6.2	0.06
Boreogadus saida	1|individual	100.7	75.9	8.4	0.66
	Size class + 1|individual	101.1	77.2	7.6	0.34

Table 3). Overall, average partitioning of basal resources was similar to that of *A. glacialis* (Fig. 4D), with iPOM dominating the contributions, minimal estimated pPOM, and *M. arctica* strands making intermediate basal resource contributions.

Distinguishing between Arctic microalgal resources

The iPOM and pPOM $\delta^{13}C_{EAA}$ values represent indiscriminate collections of microalgal species and other particles sampled in the sea-ice or at approximate 10 m depth in the open water column. Comparing the $\delta^{13}C_{EAA}$ patterns of select cultured Arctic microalgal species to those measured within the POM filtrates thus assesses whether the cultured species represent those found in the field at the time of sampling. The iPOM and pPOM $\delta^{13}C_{EAA}$ patterns grouped closely to those of cultured centric diatoms *M. arctica*, *Thalassiosira* sp., and *T. hyalina* (Fig. 5A). PCA scores from $\delta^{13}C_{EAA}$ values of the pennate diatom *Navicula* sp. differed from those of POM filters and other cultured species by displaying the highest mean-centred phenylalanine $\delta^{13}C$ values. PC3, which accounts for 8.4% of the variation, also identifies some distinctive grouping for the ice algal diatom *Thalassiosira* sp. with the highest mean-centred leucine $\delta^{13}C$ values (Fig. 5B). Interestingly, $\delta^{13}C_{EAA}$ patterns of cultured *M. arctica* in cellular suspension were distinct from those of the field-collected *M. arctica* strands. Therefore, while some $\delta^{13}C_{EAA}$ patterns of cultured diatom species reflect those of POM filters, *M. arctica* strands are not represented by its cultured equivalent and potential for more distinctive $\delta^{13}C_{EAA}$ fingerprints of microalgal species can be observed.

Discussion

We show that with $\delta^{13}C_{EAA}$ values, specific basal resources can be simultaneously traced in various Arctic organisms across benthic, pelagic, and under-ice habitats. This study presents a first-time tracing of substantial use of sub-ice algae *M. arctica* by all the selected organisms studied that cover a breadth of trophic guilds, as well as quantifying the contribution of algae-associated bacteria to Arctic sponges with their specific $\delta^{13}C_{EAA}$ fingerprints. The isotopic characterization of *M. arctica* strands and estimates of their contribution to the Arctic food webs as distinct from other microalgal groups is novel. Typically only iPOM, although often mentioned to include *M. arctica*, and pPOM are distinguished in Arctic biomarker studies (Søreide et al. 2006, 2008; Kohlbach et al. 2016; Schollmeier et al. 2018; Kunisch et al. 2021). However, the $\delta^{13}C_{EAA}$ fingerprint of *M. arctica* strands sampled in situ is unique to the natural under-ice habitat where they form long strands, compared to the $\delta^{13}C_{EAA}$ patterns of suspended *M. arctica* cells grown in culture. The disparity could be related to the mucus associated with the *M. arctica* strand ecotype (Poulin et al. 2014) producing distinctive proteins and hence $\delta^{13}C_{EAA}$ values. Bacteria are often enriched in algae aggregates (Riedel et al. 2006) and this may also change the $\delta^{13}C_{EAA}$ patterns of *M. arctica* strands. Stomach content analyses have confirmed that *M. arctica* is a food source for benthic fauna, such as holothurians and ophiuroids (Boetius et al. 2013), which is likely due to the rapid transport of *M. arctica* strands to the seafloor in spring as a result of their relatively dense mass and the weight of poorly soluble minerals (i.e., gypsum crystals) precipitated within the sea-ice brine channels (Fernández-Méndez et al. 2014; Wollenburg et al. 2020). The contribution of *M. arctica* strands to the Arctic food web could become more substantial in the near future with thinning sea-ice and subsequent increased light penetration stimulating their growth (Nicolaus et al. 2012; Boetius et al. 2013; Fernández-Méndez et al. 2014). However, in the long term, sea-ice retreat in a warming Arctic ocean is anticipated to result in the loss of this important food source with yet unpredictable consequences for benthic, pelagic, and under-ice ecosystems (Lannuzel et al. 2020).

Besides *M. arctica* strands, consistent incorporation of bacterial biomass was evident in sponges with the mixing models, suggesting limited variation in the basal resource utilization between individuals. Sponges are known to filter out bacteria associated with pelagic POM, but it is challenging to determine whether sponges actually consume the bacteria (Renaud et al. 2015; Parzanini et al. 2018) or are in symbiosis with the bacteria supplying carbon and nitrogen (Webster and Blackall 2009). Some microbes are unique to the sponge

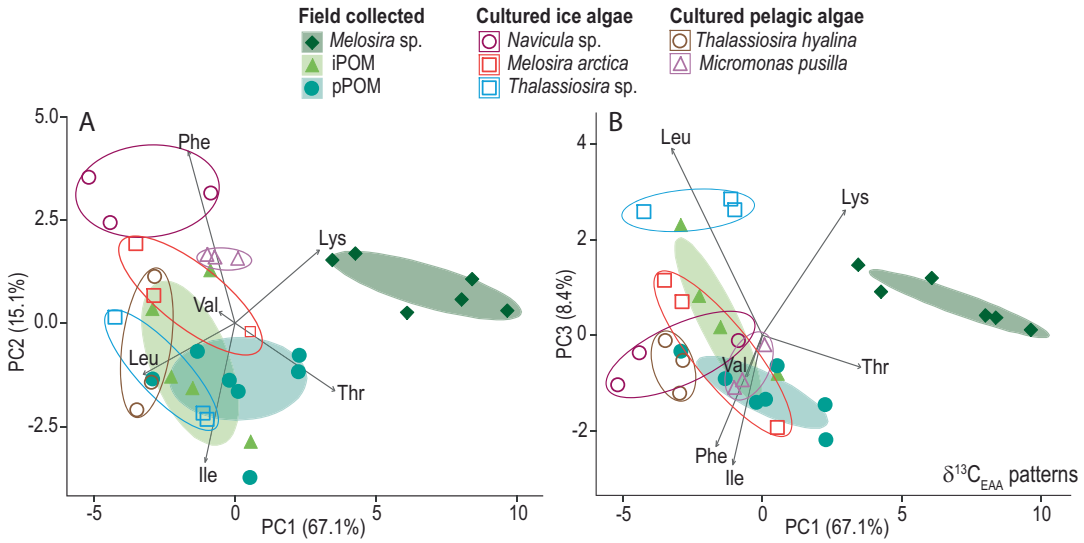

Fig. 5. Principal component analysis of the six individual mean-centred $\delta^{13}C_{EAA}$ values that comprise the $\delta^{13}C_{EAA}$ patterns in field-collected iPOM and pPOM filters compared to several laboratory cultured ice algal and pelagic phytoplankton species. Ellipses around the field-collected data represent 60% of the data, while those around the cultured microalgae species are drawn for identification purposes.

core microbiome, which are observed in related sponge species occurring in different regions, and cannot be acquired from the surrounding environment (Hentschel et al. 2002; Fiore et al. 2013). Studies on tropical sponges have identified sponge microbiomes based on distinctive $\delta^{13}C_{EAA}$ patterns or baseline $\delta^{13}C_{EAA}$ values (Macartney et al. 2020; Shih et al. 2020). However, with increasing investigations it is becoming evident that bacteria generally display significant variation in $\delta^{13}C_{EAA}$ patterns (Liew et al. 2019) and it is likely that certain microbial clades can have specific $\delta^{13}C_{EAA}$ fingerprints. Thus, for a thorough investigation it is essential to characterize all the microbial $\delta^{13}C_{EAA}$ patterns relevant to the sponge environment, core microbiome, and other non-microbial food sources. The bacterial species used in this study were isolated from Arctic sea-ice algae or phytoplankton enrichments, which indicates that they could be a food source for Arctic sponges. The collected bacteria *P. elyakovii* can cause aggregate formation in the diatom *Chaeotoceros socialis* and increase their contribution to the benthic ecosystem (Rapp et al. 2018; Vonnahme et al. 2021). As the sponge tissue represents an overall inseparable collection of undigested food items, microbiome and indigenous sponge tissue, microbial basal resources used by the sponge might be identified as those not part of the core microbiome. Other *Pseudoalteromonas* species found within Antarctic sponges are not considered to be part of the core microbiome because the bacterial species has also been detected in the water column (Savoca et al. 2019). The similarities in $\delta^{13}C_{EAA}$ patterns of the two *Pseudoalteromonas* species and the sponge tissue in this study might therefore indicate that the bacteria is a direct food source for this Arctic sponge species.

The full breadth of the diet of Arctic sea cucumbers remains largely unexplored, however, holothurians are often observed in the proximity of macroalgae and thus are fed macroalgae in aquaculture studies (Gao et al. 2011; Wen et al. 2016). Our study indicates there is potentially large individual variation in the diets of the Arctic sea cucumber with a high proportion of the kelp *L. digitata* along with *M. arctica* strands and microalgae (includes iPOM and pPOM). The direct consumption of kelp by strictly detrital feeding sea cucumbers is improbable and thus it is likely that the kelp $\delta^{13}C_{EAA}$ fingerprints were preserved in relatively fresh kelp detritus. High individual diet variability in sea cucumbers might be due to their opportunistic feeding behavior taking advantage of the available but spatiotemporally patchy detritus within their habitat range. Considering that the kelp and sea cucumbers were collected below known Arctic kelp forest depths at 67 m (Krause-Jensen et al. 2019), the consumed and collected kelp most likely originated from coastal areas. Earlier studies showed substantial export rates of kelp to deep fjord basins and shelf areas, down to deep sea habitats due to currents and storms (Krumhansl and Scheibling 2012; Ramirez-Llodra et al. 2021), but this might be the first quantitative indication of the role of kelp detritus for sea cucumbers beyond the kelp production area.

From our results, it is evident that the Arctic benthic fauna use a wide range of basal resources across bacteria, macroalgae and *M. arctica* in early Arctic spring. While broad basal resources are distinguished by large differences in $\delta^{13}C_{EAA}$ patterns, exploring finer scale differentiation between and within under-ice and pelagic microalgae groups cannot be achieved. For the benthic organisms, specific distinctions in their more limited reliance on downward fluxes of microalgae production from the overlying waters and sea-ice in conjunction with *M. arctica* strands does not necessarily impact our ecological understanding of these organisms. In contrast, however, the

crustaceans and polar cod are known to primarily rely on microalgal resources given their feeding ecology (Kohlbach et al. 2016; Eriksen et al. 2020), which is broadly supported by the close match of the $\delta^{13}C_{EAA}$ patterns in their tissue to those of the iPOM/pPOM filtrates, and *M. arctica*. However, the restricted $\delta^{13}C_{EAA}$ pattern mixing space defined by microalgal resources means statistically evaluating basal resource contributions within this space is highly sensitive to small deviations that may or may not be biologically meaningful (Phillips et al. 2014). This could be alleviated by an ability to focus on singular microalgal taxa as the primary basal resource, allowing for an exploration of the fine-scale distinctions between microalgal clades that relate to functionality or divergence. The feasibility for specific microalgae $\delta^{13}C_{EAA}$ fingerprints has become evident from the observation of fine distinctions in tissue $\delta^{13}C_{EAA}$ patterns of herring and sprat with a primary reliance on microalgae across Baltic Sea locations (Larsen et al. 2020).

Although similar, the $\delta^{13}C_{EAA}$ patterns in crustaceans and polar cod tissues were not completely represented by the microalgae resources. This is likely caused by an insufficient representation by the iPOM/pPOM filtrates of the diversity in under-ice and pelagic microalgal communities used by these consumers. The $\delta^{13}C_{EAA}$ patterns of our cultured phytoplankton shows that fine-scale distinctions within Arctic microalgae are possible, which partially explain the variation in the consumer tissue $\delta^{13}C_{EAA}$ patterns. The mean-centred phenylalanine $\delta^{13}C$ values in the tissues of the pelagic organisms were about $\sim$ 1–2‰ higher than those of the microalgae resources measured. The cultured pennate ice-diatom *Navicula* sp. in particular expressed a $\delta^{13}C_{EAA}$ pattern distinctive from those in iPOM and pPOM filtrates that directionally matched the observed elevated phenylalanine $\delta^{13}C$ values of pelagic and sympagic consumers. Conversely, the $\delta^{13}C_{EAA}$ patterns of cultured centric diatoms, in particular *Thalassiosira* species, were reflected in the iPOM/pPOM filtrate $\delta^{13}C_{EAA}$ patterns. A diatom dominance in our iPOM/pPOM filtrates was confirmed by fatty acid analysis of POM filtrates taken in parallel to ours (Kunisch et al. 2021). The Arctic microalgal species composition is known to change rapidly from a winter domination by ciliates, flagellates, and dinoflagellates which changes to diatoms in spring (Kauko et al. 2018) and is driven by environmental drivers such as nutrient status, light, water mixing regime and temperature (Ardyna and Arrigo 2020). Organisms can integrate changing basal resource isotopic compositions over several weeks during periods of microalgal blooms (Cobain et al. 2022). Therefore, ciliate and dinoflagellate production prior to early spring POM sampling could have contributed to tissue $\delta^{13}C_{EAA}$ patterns of the consumers. A more systematic and wider characterization of $\delta^{13}C_{EAA}$ patterns in Arctic microalgae in comparison to field-collected filtrates will give more insight into which extent microalgae clades can be distinguished.

The $\delta^{13}C_{EAA}$ patterns are not the only potential distinguishing factor between Arctic microalgae as baseline $\delta^{13}C_{EAA}$ values broadly display large differences between under-ice and pelagic microalgae. Despite having similar $\delta^{13}C_{EAA}$ patterns, the iPOM and pPOM were readily separated by their baseline $\delta^{13}C_{EAA}$ values, differences that are commonly attributed to carbon limitation in sympagic microalgae (de la Vega et al. 2019). The elevation in ^{13}C of iPOM compared to pPOM as observed in the baseline $\delta^{13}C_{EAA}$ values is also consistently found in carbon isotopes of bulk tissues and fatty acids, as measured during the same expedition as this study and elsewhere (Søreide et al. 2006; Kohlbach et al. 2016; de la Vega et al. 2019; Kunisch et al. 2021). These baseline $\delta^{13}C_{EAA}$ values of under-ice and pelagic microalgae, and *M. arctica* strands were reflected in the tissues of the crustaceans and polar cod (Fig. 4A). Proportional estimates of iPOM use by these organisms with baseline $\delta^{13}C_{EAA}$ values is similar to those found with bulk isotopes and isotopes of fatty acids if the use of *M. arctica* strands is included in the iPOM use. With compound-specific isotope analysis of fatty acids, iPOM use in late summer for *A. glacialis* was estimated to be 58–92%, *C. hyperboreus* 34–65%, and for *B. saida* 34–65% (Kohlbach et al. 2016, 2017). Whereas bulk isotope analyses found *A. glacialis* 90%, *C. hyperboreus* 34%, and *B. saida* 64% (Søreide et al. 2006). However, our model estimates indicated that the microalgae use was not homogenous across individuals of each species. Sampling site was important in determining the variability in basal resource reliance of *C. hyperboreus* and to a lesser extent for the ice-amphipod *A. glacialis* (Fig. 4B,C). This probably reflected spatial differences in resource availability, whereas individual variation within sampling locations was limited. Individuals of *C. hyperboreus* caught at a depth of 200 m (station 77.3) showed significantly higher pPOM proportions compared to those sampled further north where there is greater availability of iPOM derived production. Once the effect of site has been accounted for, mixing models can facilitate further interrogation of data to identify potential sources of unknown variability within individual tracers, in this case baseline $\delta^{13}C_{EAA}$ values. By removing individual effects from mixing models, residual error structures can be approximated for each EAA that indicate the extent to which the model has to "stretch" the variation in baseline $\delta^{13}C_{EAA}$ values of the basal resources to account for the variation observed in the consumer tissues. These stretch errors are expected to fall between 0 and 1 as individuals average over the variability expressed in the basal resources as they are assimilated in tissues. Stretch error values greater than 1 imply other drivers of variation unaccounted for in the mixing model (Stock and Semmens 2016; Stock et al. 2018). Our mixing models estimated acceptable stretch errors of < 1 for each EAA except for phenylalanine, which was > 2 for both consumers (Table 4). Interestingly, this aligns with the deviations observed in the mean-centred phenylalanine $\delta^{13}C$ values (Fig. S2). Examination of stretch errors in mixing models can therefore be used more generally to highlight potentially unknown processes or drivers of variation that

Table 4. Mean stretch errors (standard deviation in parentheses) for each EAA estimated for species-specific zooplankton models with site as a random factor.

Model	ξ_{VAL}	ξ_{ILE}	ξ_{LEU}	ξ_{THR}	ξ_{PHE}	ξ_{LYS}
Apherusa glacialis	0.70 (0.93)	0.89 (1.11)	0.64 (0.65)	0.75 (0.72)	2.34 (2.60)	0.98 (1.07)
Calanus hyperboreus	0.64 (0.64)	0.84 (0.94)	0.74 (0.75)	2.08 (1.81)	4.95 (3.87)	0.91 (0.83)

are specific to individual EAAs or other tracers, as they do here with phenylalanine. It is important to recognize however that the ability to interpret stretch errors is limited to specific cases where individual consumers within groups have the same diet (Stock et al. 2018).

In contrast to zooplankton species, high individual variability in microalgae use was observed for polar cod that was not attributed to body size (Fig. 4E). This implies differences in basal resource use may be linked to individual movement behaviors rather than average ontogenetic shifts in trophic ecology. We cannot completely exclude a minor reliance on kelp by polar cod, as the tissue $\delta^{13}C_{EAA}$ patterns in some individuals showed some similarity to those of kelp. Yet, the baseline $\delta^{13}C_{EAA}$ values of kelp are comparable to iPOM and thus cannot be used to calculate the reliance on kelp resources by polar cod. However, stomach content analyses in the northern Barents Sea show the polar cod's almost exclusive feeding on pelagic and sympagic zooplankton (Eriksen et al. 2020), and thus we can a priori exclude kelp having any significant contribution to *B. saida*.

This study highlights that in Arctic food web studies, certain microalgae species or even functional forms within species can potentially be distinguished with specific $\delta^{13}C_{EAA}$ fingerprints. We show this with *M. arctica*, as well as in the diatom-dominated iPOM/pPOM filtrates when compared to cultured diatom $\delta^{13}C_{EAA}$ patterns. However, a distinction with $\delta^{13}C_{EAA}$ patterns on functional group level of microalgae defined as diatoms, dinoflagellates, or ciliates that occur both in the under-ice and pelagic habitat cannot indicate their habitat origin. The baseline $\delta^{13}C_{EAA}$ values onto which $\delta^{13}C_{EAA}$ patterns are based however are indicative of the habitat origin of microalgae functional groups due to the carbon limitation in the under-ice habitat compared to the pelagic environment. The two related Arctic microalgae characterization approaches of $\delta^{13}C_{EAA}$ patterns and baseline $\delta^{13}C_{EAA}$ values thus might need to be employed in tandem to disentangle specific species or functional groups, and their habitat of origin. However, the specific microalgae characterization with $\delta^{13}C_{EAA}$ values needs to be systematically approached due to the subtle changes in Arctic microalgae species composition at the sea-ice marginal zone, where pelagic species are becoming more prevalent. Ongoing sea-ice melt and subsequent increasing under-ice light conditions benefit pelagic haptophytes such as *Phaeocystis pouchetti*, which now have under-ice blooms and progressively dominate the Arctic microalgal species composition in summer (Nöthig et al. 2015; Assmy et al. 2017). Arctic prasinophytes, such as *M. pusilla*, are also thought to increase growth rates by benefitting from warming Arctic spring conditions and ocean acidification. With a decreasing diatom dominance, these prasinophytes also might increase in biomass and importance to the Arctic food web (Hoppe et al. 2018). The potential ability to distinctly characterize these specific Arctic microalgae and trace their use by organisms in the Arctic food web with $\delta^{13}C_{EAA}$ patterns could lead to insights into whether these new basal resources are used to support the sea-ice marginal Arctic food web.

Conclusions

This study shows that specific basal resources at the sea-ice marginal zone in the northern Barents Sea can be investigated with $\delta^{13}C_{EAA}$ patterns of prominent Arctic basal resources from the under-ice, pelagic and benthic origin. The estimated substantial use of *M. arctica* strands by all the selected under-ice, pelagic and benthic fauna shows that this chain-forming diatom is an important contributor to the early Arctic spring productivity. The $\delta^{13}C_{EAA}$ fingerprints from cultured algae-associated bacteria indicated their specific use by Arctic sponges, while those of field-collected kelp and red macroalgae were linked to sea cucumbers. No significant use of the selected fungi species was detected by these benthic species. The similarity of the $\delta^{13}C_{EAA}$ patterns in the tissues of the ice-amphipods, copepods, and polar cod to those of the microalgae resources (i.e., iPOM/pPOM filtrates and *M. arctica* strands) showed their dependence on microalgae. The distinctive differences in microalgae baseline $\delta^{13}C_{EAA}$ values aligned with those in the tissues of the crustaceans and polar cod, allowed estimating their proportional use. We suggest that Arctic microalgae can be further characterized with distinctive $\delta^{13}C_{EAA}$ patterns on species or functional level when a systematic exploration of singular cultured microalgae species is performed in combination with field filtrates or collections. However, as some functional groups such as diatoms occur in both the under-ice and pelagic environment, the baseline $\delta^{13}C_{EAA}$ values need to be evaluated alongside the $\delta^{13}C_{EAA}$ fingerprints to identify their under-ice or pelagic origin. The approach has the potential to identify the specific pelagic microalgae groups that contribute to the productivity of Arctic under-ice, pelagic, and benthic food webs. This could become a powerful tool to assess whether pelagic phytoplankton that are observed to expand toward the sea-ice marginal zone with

under-ice blooms contribute to the productivity of Arctic food webs at the sea-ice marginal zone.

Data availability statement

The full dataset can be found in the data repository PANGAEA: https://doi.org/10.1594/PANGAEA.936933.

References

Ardyna, M., and K. R. Arrigo. 2020. Phytoplankton dynamics in a changing Arctic Ocean. Nat. Clim. Change **10**: 892–903. doi:10.1038/s41558-020-0905-y

Assmy, P., and others. 2017. Leads in Arctic pack ice enable early phytoplankton blooms below snow-covered sea ice. Sci. Rep. **7**: 40850. doi:10.1038/srep40850

Besser, A. C., E. A. Elliott Smith, and S. D. Newsome. 2022. Assessing the potential of amino acid $\delta^{13}C$ and $\delta^{15}N$ analysis in terrestrial and freshwater ecosystems. J. Ecol. **110**: 935–950. doi:10.1111/1365-2745.13853

Boetius, A., and others. 2013. Export of algal biomass from the melting Arctic Sea ice. Science **339**: 1430–1432. doi:10.1126/science.1231346

Budge, S. M., M. J. Wooller, A. M. Springer, S. J. Iverson, C. P. McRoy, and G. J. Divoky. 2008. Tracing carbon flow in an arctic marine food web using fatty acid-stable isotope analysis. Oecologia **157**: 117–129. doi:10.1007/s00442-008-1053-7

Cobain, M. R., R. A. McGill, and C. N. Trueman. 2022. Stable isotopes demonstrate seasonally stable benthic-pelagic coupling as newly-fixed nutrients are rapidly transferred through food chains in an estuarine fish community. J. Fish Biol. doi:10.1111/jfb.15005

Cohen, J., and others. 2014. Recent Arctic amplification and extreme mid-latitude weather. Nat. Geosci. **7**: 627–637. doi:10.1038/ngeo2234

Darnis, G., and others. 2012. Current state and trends in Canadian Arctic marine ecosystems: II. Heterotrophic food web, pelagic-benthic coupling, and biodiversity. Clim. Change **115**: 179–205. doi:10.1007/s10584-012-0483-8

de la Vega, C., C. Mahaffey, R. M. Jeffreys, R. Tuerena, and R. Ganeshram. 2019. Temporal and spatial trends in marine carbon isotopes in the Arctic Ocean and implications for food web studies. Glob. Change Biol. **25**: 4116–4130. doi:10.1111/gcb.14832

Docherty, G., V. Jones, and R. P. Evershed. 2001. Practical and theoretical considerations in the gas chromatography/combustion/isotope ratio mass spectrometry $\delta^{13}C$ analysis of small polyfunctional compounds. Rapid Commun. Mass Spectrom. **15**: 730–738. doi:10.1002/rcm.270

Elliott Smith, E. A., M. D. Fox, M. L. Fogel, and S. D. Newsome. 2022. Amino acid $\delta^{13}C$ fingerprints of nearshore marine autotrophs are consistent across broad spatiotemporal scales: An intercontinental isotopic dataset and likely biochemical drivers. Funct. Ecol. **36**: 1191–1203. doi:10.1111/1365-2435.14017

Eriksen, E., and others. 2020. Diet and trophic structure of fishes in the Barents Sea: The Norwegian-Russian program "year of stomachs" 2015—Establishing a baseline. Prog. Oceanogr. **183**: 102262. doi:10.1016/j.pocean.2019.102262

Fernández-Méndez, M., F. Wenzhöfer, I. Peeken, H. L. Sørensen, R. N. Glud, and A. Boetius. 2014. Composition, buoyancy regulation and fate of ice algal aggregates in the Central Arctic Ocean. PLoS One **9**: e107452. doi:10.1371/journal.pone.0107452

Fernández-Méndez, M., C. Katlein, B. Rabe, M. Nicolaus, I. Peeken, K. Bakker, H. Flores, and A. Boetius. 2015. Photosynthetic production in the central Arctic Ocean during the record sea-ice minimum in 2012. Biogeosciences **12**: 3525–3549. doi:10.5194/bg-12-3525-2015

Fiore, C. L., J. K. Jarett, and M. P. Lesser. 2013. Symbiotic prokaryotic communities from different populations of the giant barrel sponge, *Xestospongia muta*. Microbiology **2**: 938–952. doi:10.1002/mbo3.135

Gao, Q. F., Y. Wang, S. Dong, Z. Sun, and F. Wang. 2011. Absorption of different food sources by sea cucumber *Apostichopus japonicus* (Selenka) (Echinodermata: Holothuroidea): Evidence from carbon stable isotope. Aquaculture **319**: 272–276. doi:10.1016/j.aquaculture.2011.06.051

Gosselin, M., M. Levasseur, P. A. Wheeler, R. A. Horner, and B. C. Booth. 1997. New measurements of phytoplankton and ice algal production in the Arctic Ocean. Deep-Sea Res. II: Top. Stud. Oceanogr. **44**: 1623–1625. doi:10.1016/S0967-0645(97)00054-4

Gradinger, R. 2009. Sea-ice algae: Major contributors to primary production and algal biomass in the Chukchi and Beaufort seas during May/June 2002. Deep-Sea Res. Part II: Top. Stud. Oceanogr. **56**: 1201–1212. doi:10.1016/j.dsr2.2008.10.016

Grebmeier, J. M., K. E. Frey, L. W. Cooper, and M. Kędra. 2018. Trends in benthic macrofaunal populations, seasonal sea ice persistence, and bottom water temperatures in the Bering Strait region. Oceanography **31**: 136–151. doi:10.5670/oceanog.2018.224

Guillard, R. R. L., and J. H. Ryther. 1962. Studies of marine planktonic diatoms: I. *Cyclotella nana* (Hustedt), and *Detonula confervacae* (Cleve) gran. Can. J. Microbiol. **8**: 229–239. doi:10.1139/m62-029

Hegseth, E. N. 1998. Primary production of the northern Barents Sea. Polar Res. **17**: 113–123. doi:10.1111/j.1751-8369.1998.tb00266.x

Hentschel, U., J. Hopke, M. Horn, A. B. Friedrich, M. Wagner, J. Hacker, and B. S. Moore. 2002. Molecular evidence for a uniform microbial community in sponges from different oceans. Appl. Environ. Microbiol. **68**: 4431–4440. doi:10.1128/AEM.68.9.4431-4440.2002

Hoppe, C., C. M. Flintrop, and B. Rost. 2018. The arctic picoeukaryote *Micromonas pusilla* benefits synergistically from warming and ocean acidification. Biogeosciences **15**: 4353–4365. doi:10.5194/bg-15-4353-2018

Ji, R., M. Jin, and Ø. Varpe. 2013. Sea ice phenology and timing of primary production pulses in the Arctic Ocean. Glob. Change Biol. **19**: 734–741. doi:10.1111/gcb.12074

Kauko, H. M., and others. 2018. Algal colonization of young arctic sea ice in spring. Front. Mar. Sci. **5**: 199. doi:10.3389/fmars.2018.00199

Kędra, M., and others. 2015. Status and trends in the structure of Arctic benthic food webs. Polar Res. **339**: 23775. doi:10.3402/polar.v34.23775

Kohlbach, D., M. Graeve, B. A. Lange, C. David, I. Peeken, and H. Flores. 2016. The importance of ice algae-produced carbon in the Central Arctic Ocean ecosystem: Food web relationships revealed by lipid and stable isotope analyses. Limnol. Oceanogr. **61**: 2027–2044. doi:10.1002/lno.10351

Kohlbach, D., F. L. Schaafsma, M. Graeve, B. Lebreton, B. A. Lange, C. David, M. Vortkamp, and H. Flores. 2017. Strong linkage of polar cod (*Boreogadus saida*) to sea ice algae-produced carbon: Evidence from stomach content, fatty acid and stable isotope analyses. Prog. Oceanogr. **152**: 62–74. doi:10.1016/j.pocean.2017.02.003

Krause-Jensen, D., and others. 2019. Deep penetration of kelps offshore along the west coast of Greenland. Front. Mar. Sci. **6**: 375. doi:10.3389/fmars.2019.00375

Krumhansl, K. A., and R. E. Scheibling. 2012. Production and fate of kelp detritus. Mar. Ecol. Prog. Ser. **467**: 281–302. doi:10.3354/meps09940

Kunisch, E. H., M. Graeve, R. Gradinger, T. Haug, K. M. Kovacs, C. Lydersen, Ø. Varpe, and B. A. Bluhm. 2021. Ice-algal carbon supports harp and ringed seal diets in the European Arctic: Evidence from fatty acid and stable isotope markers. Mar. Ecol. Prog. Ser. **675**: 181–197. doi:10.3354/meps13834

Kvernvik, A. C., S. D. Rokitta, E. Leu, L. Harms, T. M. Gabrielsen, B. Rost, and C. J. M. Hoppe. 2020. Higher sensitivity towards light stress and ocean acidification in an Arctic Sea-ice-associated diatom compared to a pelagic diatom. New Phytol. **226**: 1708–1724. doi:10.1111/nph.16501

Lange, B. A., and others. 2019. Contrasting ice algae and snow-dependent irradiance relationships between first-year and multiyear sea ice. Geophys. Res. Lett. **46**: 10834–10843. doi:10.1029/2019GL082873

Lannuzel, D., and others. 2020. The future of Arctic Sea-ice biogeochemistry and ice-associated ecosystems. Nat. Clim. Change **10**: 983–992. doi:10.1038/s41558-020-00940-4

Larsen, T., D. L. Taylor, M. B. Leigh, and D. M. O'Brien. 2009. Stable isotope fingerprinting: A novel method for identifying plant, fungal, or bacterial origins of amino acids. Ecology **90**: 3526–3535. doi:10.1890/08-1695.1

Larsen, T., M. J. Wooller, M. L. Fogel, and D. M. O'Brien. 2012. Can amino acid carbon isotope ratios distinguish primary producers in a mangrove ecosystem? Rapid Commun. Mass Spectrom. **26**: 1541–1548. doi:10.1002/rcm.6259

Larsen, T., M. Ventura, N. Andersen, D. M. O'Brien, U. Piatkowski, and M. D. McCarthy. 2013. Tracing carbon sources through aquatic and terrestrial food webs using amino acid stable isotope fingerprinting. PLoS One **8**: e73441. doi:10.1371/journal.pone.0073441

Larsen, T., L. T. Bach, R. Salvatteci, Y. V. Wang, N. Andersen, M. Ventura, and M. D. McCarthy. 2015. Assessing the potential of amino acid ^{13}C patterns as a carbon source tracer in marine sediments: Effects of algal growth conditions and sedimentary diagenesis. Biogeosciences **12**: 4979–4992. doi:10.5194/bg-12-4979-2015

Larsen, T., T. Hansen, and J. Dierking. 2020. Characterizing niche differentiation among marine consumers with amino acid $\delta^{13}C$ fingerprinting. Ecol. Evol. **10**: 7768–7782. doi:10.1002/ece3.6502

Leu, E., J. E. Søreide, D. O. Hessen, S. Falk-Petersen, and J. Berge. 2011. Consequences of changing sea-ice cover for primary and secondary producers in the European Arctic shelf seas: Timing, quantity, and quality. Prog. Oceanogr. **90**: 18–32. doi:10.1016/j.pocean.2011.02.004

Liew, J. H., K. W. J. Chua, E. R. Arsenault, J. H. Thorp, A. Suvarnaraksha, A. Amirrudin, and D. C. J. Yeo. 2019. Quantifying terrestrial carbon in freshwater food webs using amino acid isotope analysis: Case study with an endemic cavefish. Methods Ecol. Evol. **10**: 1594–1605. doi:10.1111/2041-210X.13230

Lynch, A. H., N. J. Kruger, R. E. M. Hedges, and J. S. O. McCullagh. 2016. Variability in the carbon isotope composition of individual amino acids in plant proteins from different sources: 1 leaves. Phytochemistry **125**: 27–34. doi:10.1016/j.phytochem.2016.01.011

Macartney, K. J., M. Slattery, and M. P. Lesser. 2020. Trophic ecology of Caribbean sponges in the mesophotic zone. Limnol. Oceanogr. **66**: 1113–1124. doi:10.1002/lno.11668

McMahon, K. W., M. L. Fogel, T. S. Elsdon, and S. R. Thorrold. 2010. Carbon isotope fractionation of amino acids in fish muscle reflects biosynthesis and isotopic routing from dietary protein. J. Anim. Ecol. **79**: 1132–1141. doi:10.1111/j.1365-2656.2010.01722.x

McMahon, K. W., M. J. Polito, S. Abel, M. D. Mccarthy, and S. R. Thorrold. 2015. Carbon and nitrogen isotope fractionation of amino acids in an avian marine predator, the gentoo penguin (*Pygoscelis papua*). Ecol. Evol. **5**: 1278–1290. doi:10.1002/ece3.1437

Nicolaus, M., C. Katlein, J. Maslanik, and S. Hendricks. 2012. Changes in Arctic Sea ice result in increasing light transmittance and absorption. Geophys. Res. Lett. **39**: L240501. doi:10.1029/2012GL053738

Nöthig, E. M., and others. 2015. Summertime plankton ecology in Fram Strait—a compilation of long- and short-term

observations. Polar Res. **34**: 23349. doi:10.3402/polar.v34.23349

Notz, D., and J. Stroeve. 2018. The trajectory towards a seasonally ice-free Arctic Ocean. Curr. Clim. Chang. Reports **4**: 407–416. doi:10.1007/s40641-018-0113-2

Parnell, A. C., R.Inger, S. Bearhop, and A. L. Jackson. 2010. Source partitioning using stableisotopes coping with too much variation. PLoS One **5**: e9672. doi:10.1371/journal.pone.0009672

Parzanini, C., C. C. Parrish, J. F. Hamel, and A. Mercier. 2018. Trophic relationships of deep-sea benthic invertebrates on a continental margin in the NW Atlantic inferred by stable isotope, elemental, and fatty acid composition. Prog. Oceanogr. **168**: 279–295. doi:10.1016/j.pocean.2018.10.007

Phillips, D. L., R. Inger, S. Bearhop, A. L. Jackson, J. W. Moore, A. C. Parnell, B. X. Semmens, and E. J. Ward. 2014. Best practices for use of stable isotope mixing models in food-web studies. Can. J. Zool. **92**: 823–835. doi:10.1139/cjz-2014-0127

Poulin, M., G. J. C. Underwood, and C. Michel. 2014. Sub-ice colonial *Melosira arctica* in Arctic first-year ice. Diatom Res. **29**: 213–221. doi:10.1080/0269249X.2013.877085

R Core Team. 2018. R: A language and environment for statistical computing. Vienna: R Foundation for Statistical Computing. https://www.R-project.org.

Ramirez-Llodra, E., and others. 2021. Community structure of deep fjord and shelf benthic fauna receiving different detrital kelp inputs in northern Norway. Deep-Sea Res. I: Oceanogr. Res. Pap. **168**: 103433. doi:10.1016/j.dsr.2020.103433

Rapp, J. Z., M. Fernández-Méndez, C. Bienhold, and A. Boetius. 2018. Effects of ice-algal aggregate export on the connectivity of bacterial communities in the central Arctic Ocean. Front. Microbiol. **9**: 1035. doi:10.3389/fmicb.2018.01035

Renaud, P. E., T. S. Løkken, L. L. Jørgensen, J. Berge, and B. J. Johnson. 2015. Macroalgal detritus and food-web subsidies along an Arctic fjord depth-gradient. Front. Mar. Sci. **2**: 31. doi:10.3389/fmars.2015.00031

Riedel, A., C. Michel, and M. Gosselin. 2006. Seasonal study of sea-ice exopolymeric substances on the Mackenzie shelf: Implications for transport of sea-ice bacteria and algae. Aquat. Microb. Ecol. **45**: 195–206. doi:10.3354/ame045195

Ruess, L., and D. C. Müller-Navarra. 2019. Essential biomolecules in food webs. Front. Ecol. Evol. **7**: 269. doi:10.3389/fevo.2019.00269

Savoca, S., A. Lo Giudice, M. Papale, S. Mangano, C. Caruso, N. Spanò, L. Michaud, and C. Rizzo. 2019. Antarctic sponges from the Terra Nova Bay (Ross Sea) host a diversified bacterial community. Sci. Rep. **9**: 16135. doi:10.1038/s41598-019-52491-0

Schollmeier, T., A. C. M. Oliveira, M. J. Wooller, and K. Iken. 2018. Tracing Sea ice algae into various benthic feeding types on the Chukchi Sea shelf. Polar Biol. **41**: 207–224. doi:10.1007/s00300-017-2182-4

Scott, J. H., D. M. O'Brien, D. Emerson, H. Sun, G. D. McDonald, A. Salgado, and M. L. Fogel. 2006. An examination of the carbon isotope effects associated with amino acid biosynthesis. Astrobiology **6**: 867–880. doi:10.1089/ast.2006.6.867

Shih, J. L., K. E. Selph, C. B. Wall, N. J. Wallsgrove, M. P. Lesser, and B. N. Popp. 2020. Trophic ecology of the tropical Pacific sponge *Mycale grandis* inferred from amino acid compound-specific isotopic analyses. Microb. Ecol. **79**: 495–510. doi:10.1007/s00248-019-01410-x

Søreide, J. E., H. Hop, M. L. Carroll, S. Falk-Petersen, and E. N. Hegseth. 2006. Seasonal food web structures and sympagic—Pelagic coupling in the European Arctic revealed by stable isotopes and a two-source food web model. Prog. Oceanogr. **71**: 59–87. doi:10.1016/j.pocean.2006.06.001

Søreide, J. E., S. Falk-Petersen, E. N. Hegseth, H. Hop, M. L. Carroll, K. A. Hobson, and K. Blachowiak-Samolyk. 2008. Seasonal feeding strategies of *Calanus* in the high-Arctic Svalbard region. Deep-Sea Res. II: Top. Stud. Oceanogr. **55**: 2225–2244. doi:10.1016/j.dsr2.2008.05.024

Stock, B. C., and B. X. Semmens. 2016. Unifying error structures in commonly used biotracer mixing models. Ecology **97**: 2562–2569. doi:10.1002/ecy.1517

Stock, B. C., A. L. Jackson, E. J. Ward, A. C. Parnell, D. L. Phillips, and B. X. Semmens. 2018. Analyzing mixing systems using a new generation of Bayesian tracer mixing models. PeerJ **6**: e5096. doi:10.7717/peerj.5096

Sweeting, C. J., J. T. Barry, N. V. C. Polunin, and S. Jennings. 2007. Effects of body size and environment on diet-tissue $\delta^{13}C$ fractionation in fishes. J. Exp. Mar. Biol. Ecol. **352**: 165–176. doi:10.1016/j.jembe.2007.07.007

Takizawa, Y., Y. Takano, B. Choi, P. S. Dharampal, S. A. Steffan, N. O. Ogawa, N. Ohkouchi, and Y. Chikaraishi. 2020. A new insight into isotopic fractionation associated with decarboxylation in organisms: Implications for amino acid isotope approaches in biogeoscience. Prog. Earth Planet. Sci. **7**: 50. doi:10.1186/s40645-020-00364-w

Tamelander, T., M. Reigstad, H. Hop, M. L. Carroll, and P. Wassmann. 2008. Pelagic and sympagic contribution of organic matter to zooplankton and vertical export in the Barents Sea marginal ice zone. Deep-Sea Res. II: Top. Stud. Oceanogr. **55**: 2330–2339. doi:10.1016/j.dsr2.2008.05.019

Tamelander, T., C. Kivimäe, R. G. J. Bellerby, P. E. Renaud, and S. Kristiansen. 2009. Base-line variations in stable isotope values in an Arctic marine ecosystem: Effects of carbon and nitrogen uptake by phytoplankton. Hydrobiologia **630**: 63–73. doi:10.1007/s10750-009-9780-2

Tedesco, L., M. Vichi, and E. Scoccimarro. 2019. Sea-ice algal phenology in a warmer arctic. Sci. Adv. **5**: eaav4830. doi:10.1126/sciadv.aav4830

Van Franeker, J. A., Flores, H., and Van Dorssen, M. The Surface and Under Ice Trawl (SUIT). In: Flores H (ed). 2009. Frozen Desert Alive - The role of sea ice for pelagic macrofauna and its predators. PhD thesis. University of Groningen: Groningen: 181–188.

Vonnahme, T. R., and others. 2021. Modeling silicate-nitrate-ammonium co-limitation of algal growth and the importance of bacterial remineralization based on an experimental Arctic coastal spring bloom culture study. Biogeosciences **18**: 1719–1747. doi:10.5194/bg-18-1719-2021

Walsh, R. G., S. He, and C. T. Yarnes. 2014. Compound-specific $\delta^{13}C$ and $\delta^{15}N$ analysis of amino acids: A rapid, chloroformate-based method for ecological studies. Rapid Commun. Mass Spectrom. **28**: 96–108. doi:10.1002/rcm.6761

Wang, S. W., S. M. Budge, K. Iken, R. R. Gradinger, A. M. Springer, and M. J. Wooller. 2015. Importance of sympagic production to Bering Sea zooplankton as revealed from fatty acid-carbon stable isotope analyses. Mar. Ecol. Prog. Ser. **518**: 31–50. doi:10.3354/meps11076

Wang, Y. V., A. H. L. Wan, E. Lock, N. Andersen, C. Winterschuh, and T. Larsen. 2018. Know your fish: A novel compound-specific isotope approach for tracing wild and farmed salmon. Food Chem. **256**: 380–389. doi:10.1016/j.foodchem.2018.02.095

Wassmann, P., and others. 2006. Food webs and carbon flux in the Barents Sea. Prog. Oceanogr. **71**: 232–287. doi:10.1016/j.pocean.2006.10.003

Webster, N. S., and L. L. Blackall. 2009. What do we really know about sponge-microbial symbioses. ISME J. **3**: 1–3. doi:10.1038/ismej.2008.102

Welch, H. E., M. A. Bergmann, T. D. Siferd, K. A. Martin, M. F. Curtis, R. E. Crawford, R. J. Conover, and H. Hop. 1992. Energy flow through the marine ecosystem of the Lancaster sound region, Arctic Canada. Arctic **45**: 343–357. doi:10.14430/arctic1413

Wen, B., Q. F. Gao, S. L. Dong, Y. R. Hou, and H. B. Yu. 2016. Utilization of different macroalgae by sea cucumber *Apostichopus japonicus* revealed by carbon stable isotope analysis. Aquac. Environ. Interact. **8**: 171–178. doi:10.3354/AEI00173

Wollenburg, J. E., M. Iversen, C. Katlein, T. Krumpen, M. Nicolaus, G. Castellani, I. Peeken, and H. Flores. 2020. New observations of the distribution, morphology and dissolution dynamics of cryogenic gypsum in the Arctic Ocean. Cryosphere **14**: 1795–1808. doi:10.5194/tc-14-1795-2020

Acknowledgments

This study was cofunded by the Natural Environment Research Council (NERC) under the grant number NE/R012520 and the German Federal Ministry of Education and Research (BMBF) with project number 03F0800A in the joint funding scheme of Changing Arctic Oceans. K.V. and H.F. were also funded by the Helmholtz Association's Programme Oriented Funding Period 4 (POF-4), subtopic 6.1 and 6.3. We thank the captain, crew, and science teams of the RV 'Polarstern' expedition PS106 (expedition grant AWI_PS106_00). We also thank Dr. Thomas Larsen for providing practical background and discussion on the cultivation of the microorganisms and the data treatment. A special thanks goes to Dr. Paul Sargent Bray from the University of Southampton who managed the GC-IRMS laboratory. Open Access funding enabled and organized by Projekt DEAL.

Conflict of Interest

None declared.

Submitted 19 March 2022
Revised 19 October 2022
Accepted 18 January 2023

Associate editor: Peter Hernes